Atomistic model analysis of the spin reorientation transition in $(Nd_{1-x}Dy_x)_2Fe_{14}B$ systems

Masamichi Nishino,[1,*] Rachida Lamouri,[1] and Hisazumi Akai[2]

[1] *Research Center for Materials Nanoarchitectonics, National Institute for Materials Science, 1-1 Namiki, Tsukuba, Ibaraki 305-0044, Japan*

[2] *Graduate School of Engineering, Osaka University, 2-1 Yamadaoka, Suita, Osaka 565-0871, Japan*

(Dated: January 27, 2026)

Neodymium (Nd) magnets ($Nd_2Fe_{14}B$) are important permanent magnets due to their strong coercive force, which contributes to high-efficiency energy conversion technologies. This coercivity is often enhanced by substituting dysprosium (Dy). Therefore, understanding the magnetic properties of Dy-substituted systems, $(Nd_{1-x}Dy_x)_2Fe_{14}B$, is essential. We investigate the spin reorientation transition in $(Nd_{1-x}Dy_x)_2Fe_{14}B$ using a recently developed atomistic modeling approach. This modeling method captures the microscopic mechanisms of magnetic interactions and temperature effects, including thermal fluctuations. We study the x dependence of the spin reorientation transition temperature ($T_{\rm SR}$) and the canting angle (θ) of the total magnetization using an importance-sampling Monte Carlo method, based on a model with microscopic parameters derived primarily from first-principles calculations. Our estimates of $T_{\rm SR}$ and θ are consistent with experimental results. We also compare our results with those obtained from a previous mean-field-like study and show significant differences, particularly at higher Dy concentrations. Our model more accurately captures experimental trends in this regime. We attribute this improvement to more accurate representations of canting angles and anisotropy energies of the constituent atoms. Additionally, we investigate an anomalous behavior in the total magnetization of $(Nd_{1-x}Dy_x)_2Fe_{14}B$. We find a non-differentiable point in the magnetization at $T_{\rm SR}$, which becomes more pronounced with increasing x, peaking at $x = 0.5$. We discuss the origin of this anomaly in detail through analysis of the magnetic properties of the constituent atoms.

I. INTRODUCTION

Controlling the magnetic properties of permanent magnets is crucial for achieving high energy conversion efficiency. Neodymium (Nd) magnets [1–10], whose main phase is $Nd_2Fe_{14}B$, are particularly important due to their high coercive fields [11–20]. These magnets are widely used in motors, generators, electronic devices, and other applications. The increasing demand for electric vehicle motors and related technologies is expected to further expand the applications of Nd magnets.

However, Nd magnets suffer from reduced coercivity at elevated temperatures. To overcome this issue, heavy rare-earth elements such as dysprosium (Dy) are often added to enhance coercivity for practical use. The formation of Dy-rich shells, specifically $(Nd_{1-x}Dy_x)_2Fe_{14}B$, plays a key role in improving coercivity [21–27]. Therefore, investigating the magnetic properties of $(Nd_{1-x}Dy_x)_2Fe_{14}B$ is of great significance.

Theoretical studies of the magnetic properties of permanent magnets have often been conducted using continuum models [28], which rely on a small number of macroscopic magnetic parameters such as the exchange stiffness constant (A) and magnetic anisotropy energy (K). While these models are advantageous for simulating large systems, they inherently ignore microscopic details of the crystal structure and magnetic interactions due to coarse graining. Furthermore, as shown in Ref. [29], continuum models struggle to accurately incorporate temperature effects and thermal fluctuations.

Temperature-dependent properties of $R_2Fe_{14}B$ compounds have also been studied using mean-field (MF) approximations [30, 31]. However, MF approaches often yield inaccurate magnetic properties because of oversimplified modeling and the neglect of thermal fluctuations.

Recently, atomistic modeling approaches have been developed to investigate the detailed magnetic properties of permanent magnets. These models account for microscopic magnetic interactions that reflect the atomic-scale crystal structure. They also allow for an accurate treatment of temperature effects, including thermal fluctuations and the dynamics toward thermal equilibrium [32, 33]. Given the structural and interactional complexity of $R_2Fe_{14}B$ compounds, atomistic modeling is particularly well suited for studying their magnetic properties. Atomistic model studies have successfully elucidated both qualitative and quantitative aspects of Nd magnets at zero and finite temperatures [17, 34–51].

We recently investigated the thermodynamic properties of $Dy_2Fe_{14}B$ using an atomistic model [52] and compared them with those of $Nd_2Fe_{14}B$, finding good agreement with experimental results. We also studied the mechanism of coercivity enhancement due to Dy substitution in Nd magnets [49]. Our findings indicate that the crystal electric field energy barrier of Dy atoms is more resistant to thermal fluctuations at high temperatures, which contributes to the coercivity enhancement, in addition to the difference in the magnetic interaction between rare earth and iron atoms, that is, antiferro-

* Corresponding author: nishino.masamichi@nims.go.jp

magnetic coupling between Dy and Fe moments while ferromagnetic coupling between Nd and Fe moments.

$Nd_2Fe_{14}B$ exhibits a spin reorientation (SR) transition at a low temperature, which has been extensively studied [7–9, 53–58]. The SR transition in $(Nd_{1-x}Dy_x)_2Fe_{14}B$ has also attracted attention [54, 57, 59]. In this study, we focus on the SR transition in these compounds. The only theoretical analysis available for the x-dependent behavior is a mean-field-like model by Lim et al. [54], which considered Nd, Dy, and Fe in a fitted mean-field framework without employing a self-consistent field method. Here, we study the x-dependent magnetic properties related to the SR transition using an atomistic modeling approach. We show that our estimates of the SR transition temperature, $T_{\rm SR}$, and the canting angle of the total magnetic moment, θ, as functions of x are consistent with experimental observations [54, 57]. We also highlight discrepancies at large x between our results and those of Lim et al.'s MF-like method [54], and provide a detailed discussion of these differences.

Furthermore, we investigate an anomalous phenomenon in the magnetization near $T_{\rm SR}$. This anomaly was first reported by Hirosawa in $Nd_2Fe_{14}B$ [7]. However, its x-dependence has not been systematically studied. Here, we clarify this behavior using the atomistic modeling. We find that the anomaly in total magnetization becomes more pronounced with increasing x, peaks at $x = 0.5$, and then decreases. We attribute the anomaly to unusual behavior of the Nd magnetic moments.

The rest of this paper is organized as follows. In Sec. II, we describe the atomistic model. Section III presents the method to study thermodynamic quantities. In Sec. IV A, we investigate the magnetic properties of the SR transition. In Sec. IV B, we analyze the canting angles of magnetic moments. In Sec. IV C, we explore the origin of the anomalous magnetization behavior. Finally, Sec. V provides a summary of our findings.

II. MODEL

We employ the following atomistic Hamiltonian for the $(Nd_{1-x}Dy_x)_2Fe_{14}B$ system:

$$\mathcal{H} = -\sum_{i<j} 2J_{ij}\boldsymbol{s}_i\cdot\boldsymbol{s}_j - \sum_{i}^{\rm Fe} D_i(s_i^z)^2 + \sum_{i}^{\rm Nd,Dy}\sum_{l,m}\Theta_{l,i}A_{l,i}^m\langle r^l\rangle_i\hat{O}_{l,i}^m \tag{1}$$

Here, J_{ij} denotes the exchange interaction between the ith and jth atoms. D_i represents the anisotropy constant for the ith Fe atom. The third term corresponds to the crystal electric field (CEF) energy of the rare-earth atoms (Nd and Dy), where $\Theta_{l,i}$, $A_{l,i}^m$, $\langle r^l\rangle_i$, and $\hat{O}_{l,i}^m$ denote the Stevens factor, the coefficient of the spherical harmonics of the crystalline electric field, the radial expectation value, and the Stevens operator, respectively. We consider $l = 2, 4, 6$ and $m = 0$ (diagonal operators), which are the dominant contributions.

For Fe and B atoms, $\boldsymbol{s}_i$ represents the magnetic moment at site i. For Nd and Dy atoms, $\boldsymbol{s}_i$ represents the moment of the valence ($5d$ and $6s$) electrons, which are strongly coupled to the $4f$ electron moment, $\boldsymbol{\mathcal{J}}_i = g_{\rm T}\boldsymbol{J}_i\mu_{\rm B}$, where $g_{\rm T}$ is the Lande g-factor and $\boldsymbol{J}_i$ is the total angular momentum. The total moment for each rare-earth atom is given by $\boldsymbol{S}_i = \boldsymbol{s}_i + \boldsymbol{\mathcal{J}}_i$. For Nd atoms, $J = \mathcal{L} - \mathcal{S} = 9/2$ and $g_{\rm T} = 8/11$, where $\mathcal{L}$ and $\mathcal{S}$ are the orbital and spin angular momenta, respectively. For Dy atoms, $J = \mathcal{L} + \mathcal{S} = 15/2$ and $g_{\rm T} = 4/3$. For Fe and B atoms, we define $\boldsymbol{S}_i = \boldsymbol{s}_i$. It should be noted that $\boldsymbol{s}_i$ of a Nd or Dy atom and $\boldsymbol{S}_i(= \boldsymbol{s}_i)$ of an Fe atom are antiferromagnetically coupled. However, the total moment $\boldsymbol{S}_i$ of a Nd atom is ferromagnetically coupled to that of an Fe atom, whereas that of a Dy atom is antiferromagnetically coupled to Fe [49].

Monte Carlo simulations are performed to investigate thermodynamical properties of the $(Nd_{1-x}Dy_x)_2Fe_{14}B$ system as a function of x. Since x represents the concentration of Dy atoms among the rare-earth sites, larger systems are needed to accurately evaluate thermodynamic quantities for a random distribution of Dy atoms. In this study, we adopt a system consisting of 14,688 atoms, corresponding to $6\times6\times6$ unit cells with periodic boundary conditions.

First, magnetic moments and exchange interactions for $Nd_2Fe_{14}B$ and $Dy_2Fe_{14}B$ are estimated with the AkaiKKR code based on the Korringa-Kohn-Rostoker (KKR) first-principles method [60], using a single unit cell structure of each compound with periodic boundary conditions. The Liechtenstein method [61] is employed to estimate J_{ij}. In the calculations, standard muffin-tin-type potentials and the local density approximation are used. For the electronic states of the rare-earth elements, the open-core approximation is applied. The obtained data are summarized in Figs. S1–S3 of the Supplemental Material (SM) [62]. Accurate first-principles estimation of J_{ij} in $R_2Fe_{14}B$ remains challenging [63]. The applicability of the AkaiKKR method to $R_2Fe_{14}B$ has been examined and is generally regarded as reasonable [52, 63]. Magnetization values calculated using this method show agreement with experimental measurements. Although the Curie temperatures are somewhat overestimated, the dependence on R reproduces the experimental trend. These results support the validity of this method for $R_2Fe_{14}B$.

Because the system containing 14,688 atoms is too large to directly compute magnetic moments and exchange interactions using the first-principles method, we adopt the following strategy to determine the exchange interactions:
For Nd–Nd, Nd–Fe, and Nd–B bonds, we use values estimated in $Nd_2Fe_{14}B$. For Dy–Dy, Dy–Fe, and Dy–B bonds, we use values from $Dy_2Fe_{14}B$. For Nd–Dy bonds, we use the average of the Nd–Nd and Dy–Dy values. For

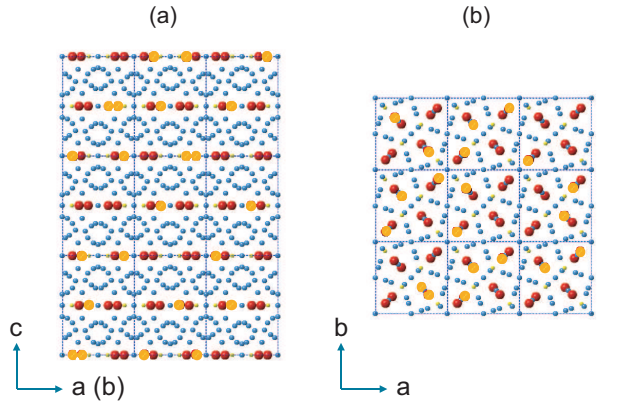

FIG. 1. (a) Side view and (b) top view of the model structure of $(Nd_{1-x}Dy_x)_2Fe_{14}B$, illustrated for a $3 \times 3 \times 3$ supercell as an expample. Red, orange, blue, and yellow spheres represent Nd, Dy, Fe, and B atoms, respectively. Lattice constants for $Nd_2Fe_{14}B$ are $l_a = l_b = 8.80$ Å and $l_c = 12.20$ Å, and for $Dy_2Fe_{14}B$ are $l_a = l_b = 8.76$ Å and $l_c = 12.01$ Å.

Fe–Fe, B–B, and Fe–B bonds, we use a weighted average of the values from $Nd_2Fe_{14}B$ and $Dy_2Fe_{14}B$, with a ratio of $1 - x$ to x for each bond. Since the corresponding exchange interaction values in $Nd_2Fe_{14}B$ and $Dy_2Fe_{14}B$ are very close (see Fig. S1– Fig. S3 in SM), this strategy is expected to be a good approximation.

For computing magnetizations, we use $\boldsymbol{s}_i$ values from $Nd_2Fe_{14}B$ and $Dy_2Fe_{14}B$ for Nd and Dy atoms, respectively. For Fe and B atoms, $\boldsymbol{s}_i$ is determined by a weighted average of the values from $Nd_2Fe_{14}B$ and $Dy_2Fe_{14}B$ using the ratio $1 - x : x$. The values of s_i for Fe and B atoms are also very close in both systems, supporting the validity of this approximation. For rare-earth atoms, A_l^m values reported by Yamada et al. [53] for $R_2Fe_{14}B$ are used, along with $\langle r^l \rangle$ from Ref. [64]. The R ions occupy the Wyckoff 4f and 4g sites. In accordance with Yamada et al. [53], the same set of CEF coefficients is employed for both positions. Determining the difference between the CEF coefficients at the 4f and 4g sites is a nontrivial problem, with published estimates ranging from negligible to appreciable [6]. Consequently, this work does not address the possible differences in the CEF energy between the two sites. The anisotropy constants D_i for six types of Fe sites are taken from first-principles results reported in Ref. [65]. The parameter values for the CEF coefficients and the anisotropy energies of Fe atoms are given in Tables S1–S3 in the SM. The anisotropy energies of Nd and Dy atoms are expected to be nearly unaffected by substitution, as these atoms are surrounded by Fe atoms, with the $4f$ electrons contributing to anisotropy and the $5d/6s$ electrons mainly contributing to exchange interactions.

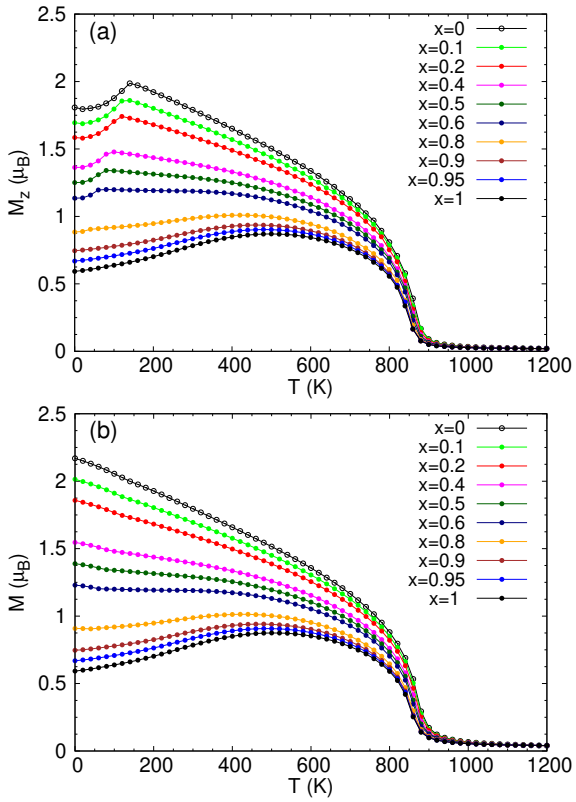

FIG. 2. Temperature dependences of (a) the z-component of the total magnetization M_z and (b) the total magnetization magnitude M for $(Nd_{1-x}Dy_x)_2Fe_{14}B$ systems over the full temperature range.

III. METHOD

We use a Metropolis importance-sampling Monte Carlo (MC) method to study equilibrium magnetizations at finite temperatures. The per-site magnetizations M_z, M_{xy}, and M for the $(Nd_{1-x}Dy_x)_2Fe_{14}B$ model are defined as

$$M_z = \frac{1}{N}\left\langle \left| \sum_{i=1}^{N} S_i^z \right| \right\rangle, \tag{2}$$

$$M_{xy} = \frac{1}{N}\left\langle \sqrt{\left(\sum_{i=1}^{N} S_i^x\right)^2 + \left(\sum_{i=1}^{N} S_i^y\right)^2} \right\rangle, \tag{3}$$

and

$$M = \frac{1}{N}\left\langle \sqrt{\left(\sum_{i=1}^{N} S_i^x\right)^2 + \left(\sum_{i=1}^{N} S_i^y\right)^2 + \left(\sum_{i=1}^{N} S_i^z\right)^2} \right\rangle, \tag{4}$$

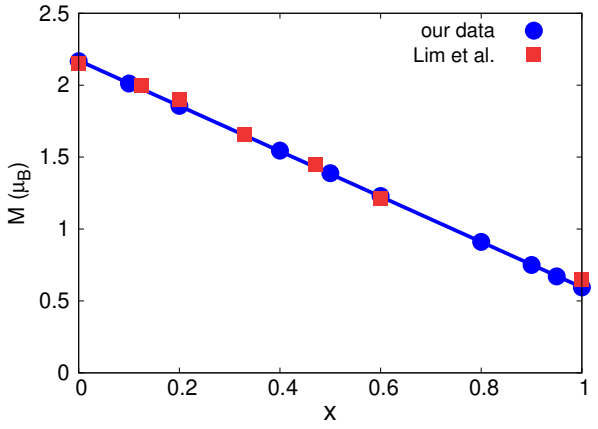

FIG. 3. Magnetization M of $(Nd_{1-x}Dy_x)_2Fe_{14}B$ systems (blue circles) as a function of concentration x at $T = 4$ K. The blue solid line represents a linear fit using the least-squares method. Red squares indicate experimental values of M at $T = 4.2$ K reported by Lim et al. [54].

, respectively. Here, N is the number of all atoms (all spins) in the $(Nd_{1-x}Dy_x)_2Fe_{14}B$ model, and $\langle\rangle$ denotes thermal average.

We also define species-specific magnetizations for Nd, Dy, and Fe atoms.

$$m(\mathrm{A}) = \frac{1}{N_\mathrm{A}} \left\langle \sqrt{\left(\sum_{i=1}^{N_\mathrm{A}} S_i^x\right)^2 + \left(\sum_{i=1}^{N_\mathrm{A}} S_i^y\right)^2 + \left(\sum_{i=1}^{N_\mathrm{A}} S_i^z\right)^2} \right\rangle, \tag{5}$$

where A denotes Nd, Dy, or Fe and N_A is the number of atom A in the $(Nd_{1-x}Dy_x)_2Fe_{14}B$ model.

We perform 200,000 Monte Carlo steps (MCS) for equilibration, followed by 400,000 to 1,600,000 MCS for measurements, with more steps applied near the SR temperature. Figures 1(a) and (b) show the side and top views, respectively, of the model structure of $(Nd_{1-x}Dy_x)_2Fe_{14}B$ for a $3 \times 3 \times 3$ supercell as an example.

IV. RESULTS

A. Spin reorientation transition

The temperature (T) dependences of M_z and M for $(Nd_{1-x}Dy_x)_2Fe_{14}B$ systems are shown in Figs. 2 (a) and (b), respectively. A cusp appears at $T_\mathrm{SR} \simeq 134$ K in the M_z–T curve for $x = 0$ ($Nd_2Fe_{14}B$), indicating a spin reorientation (SR) transition. As x increases, the cusp in M_z becomes broader and the SR transition temperature, T_SR, becomes lower. Both M and M_z decrease with increasing of x, especially at lower temperatures. Although

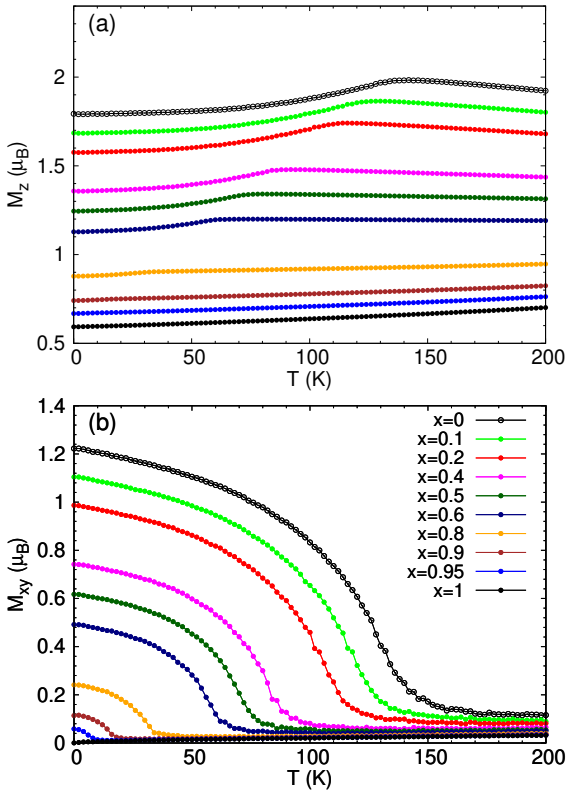

FIG. 4. Temperature dependences of (a) M_z and (b) M_{xy} for $(Nd_{1-x}Dy_x)_2Fe_{14}B$ systems at low temperatures.

M appears to change smoothly with temperature at this scale in Fig. 2(b), careful inspection around T_SR reveals that T_SR is a non-differentiable point. This feature is discussed in Sec. IV C.

Experimentally, T_SR for $Nd_2Fe_{14}B$ has been reported to range from 126 to 150 K [7–9, 53–57], and it decreases with increasing x [54, 57]. Our simulation results are consistent with these observations. The Curie temperature T_c remains almost constant with x due to the similarity in $2J_{ij}\boldsymbol{s}_i \cdot \boldsymbol{s}_j$ values between $Nd_2Fe_{14}B$ and $Dy_2Fe_{14}B$ (see Fig. S1–Fig. S3 in SM). Our estimated $T_\mathrm{c} \simeq 870$ K is a little overestimated compared to experimental values (~ 600 K) [4, 6, 7], due to a small overestimation in J_{ij}. The validity of the estimation by AkaiKKR has been discussed [52, 63]. The estimated Curie temperatures are a little overestimated, but the R dependence captures the experimental trend. The calculated magnetization of $R_2Fe_{14}B$ generally agrees with experimental values. In this paper, we focus on magnetic properties associated with the SR transition.

Figure 3 shows the concentration (x) dependence of magnetization M for $(Nd_{1-x}Dy_x)_2Fe_{14}B$ systems at $T = 4$ K. We find that M exhibits a linear dependence on x. Experimentally measured values of M at $T = 4.2$ K,

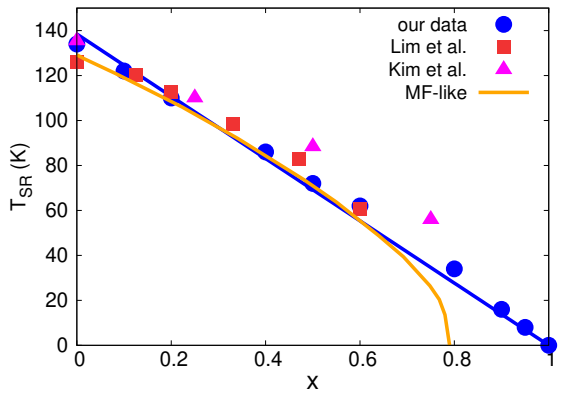

FIG. 5. Concentration (x) dependence of the spin reorientation transition temperature ($T_{\rm SR}$) for $(Nd_{1-x}Dy_x)_2Fe_{14}B$ systems (blue circles). Blue solid line is a linear fitting using the least squares method. Experimental data from Lim et al. [54] and Kim et al. [57] are shown by red squares and magenta triangles, respectively.

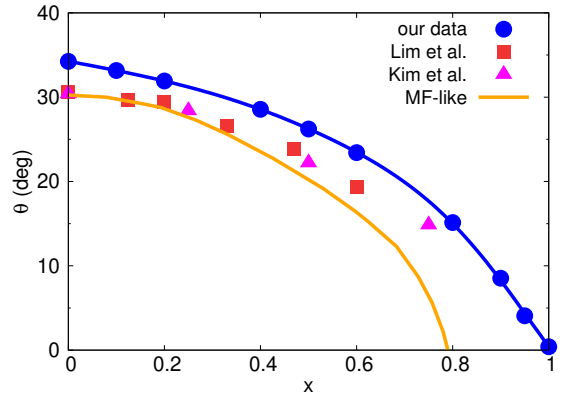

FIG. 6. Canting angle (θ) of the total magnetic moment from the c axis as a function of concentration (x) for $(Nd_{1-x}Dy_x)_2Fe_{14}B$ systems at $T = 4\,\mathrm{K}$ (blue circles). Experimental data at $T = 4.2\,\mathrm{K}$ from Lim et al. [54] and Kim et al. [57] are shown by red squares and magenta triangles, respectively. The MF-like theoretical prediction by Lim et al. [54] is also plotted as an orange solid line.

reported by Lim. et al. [54], are also plotted for comparison. We find that our estimation is in good agreement with the experimental values. Figures 4 (a) and (b) show detailed profiles of M_z and M_{xy} near the SR transition point, respectively. It is difficult to identify the SR transition for large x solely from the M_z–T curve. However, by analyzing the M_{xy}–T curve, the SR transition temperature $T_{\rm SR}$ can be clearly detected as a function of x. Notably, the SR transition is observed even for small Nd concentrations, down to $x = 0.95$.

Figure 5 illustrates the concentration (x) dependence of $T_{\rm SR}$ for $(Nd_{1-x}Dy_x)_2Fe_{14}B$ systems. We find that $T_{\rm SR}$ decreases approximately linearly with increasing x. A linear fit obtained by the least squares method, constrained to pass through the point ($x = 1, T_{\rm SR} = 0\,\mathrm{K}$), is shown by the blue solid line and serves as a good approximation to our simulation results (blue circles). Experimental values of $T_{\rm SR}$ for $x \leq 0.6$ reported by Lim et al. [54] and those for $x \leq 0.75$ reported by Kim et al. [57] are shown by red squares and magenta triangles, respectively. In addition, an estimation of $T_{\rm SR}$ as a function of x using a "MF-like" approach by Lim et al. is also given in Fig. 5 as a reference [54]. In their approach, three-sites, i.e., Nd, Dy, and Fe sites were considered under several assumptions. The temperature dependences of the anisotropy constant of the Fe site and its moment $m_{\rm Fe}$ were assumed to be similar to that in $Y_2F_{14}B$, with a modification due to the difference in the Curie temperature, where Y ions is non magnetic. The molecular-field vector $\boldsymbol{H}$ (T) at the Nd site and $\boldsymbol{H}'$ (T) at the Dy site were antiparallel and proportional to the Fe moment vector $\boldsymbol{m}_{\rm Fe}$, in which the R-R interaction was ignored. The values of H and H' at 0 K were adjustable parameters. The total magnetization was determined by the condition that the total free energy should be minimum with respect to the polar angle of $\boldsymbol{m}_{\rm Fe}$ for zero external field. Therefore, unlike a usual MF theory based on self consistent field equations, their method is a phenomenological treatment using effective fields for Nd, Dy, and Fe sites.

We find that our estimation of $T_{\rm SR}$ is close to the experimental values by Lim et al. and reasonably consistent with those by Kim et al. In Lim's MF-like result, $T_{\rm SR}$ decreases with increasing x and after $x \simeq 0.7$, it rapidly drops, reaching $T_{\rm SR} = 0$ at $x \simeq 0.79$. Our simulation result differs from the MF-like result, especially in the high x regime. In Kim's experiment, $T_{\rm SR} \simeq 56\,\mathrm{K}$ at $x = 0.75$ was given. This temperature is much larger than $T_{\rm SR} \simeq 26\,\mathrm{K}$ of the MF-like estimate. Our estimate, $T_{\rm SR} \simeq 35\,\mathrm{K}$, lies between these two values. In the next subsection, we investigate the canting angle of the total moment and discuss its characteristics.

B. Feature of canting angle

Figure 6 depicts the concentration (x) dependence of the canting angle (θ) of the total magnetic moment from the c axis for $(Nd_{1-x}Dy_x)_2Fe_{14}B$ systems at $T = 4\,\mathrm{K}$, calculated using the following relation:

$$\theta = \tan^{-1}\frac{M_{xy}}{M_z}. \tag{6}$$

Experimental data at $T = 4.2\,\mathrm{K}$ by Lim et al. [54] and Kim et al. [57] are also plotted, along with a MF-like estimation by Lim et al. [54] (orange solid line) for comparison.

The canting angle of the total moment in $Nd_2Fe_{14}B$, i.e., $x = 0$, has been experimentally estimated to be $\theta \simeq$

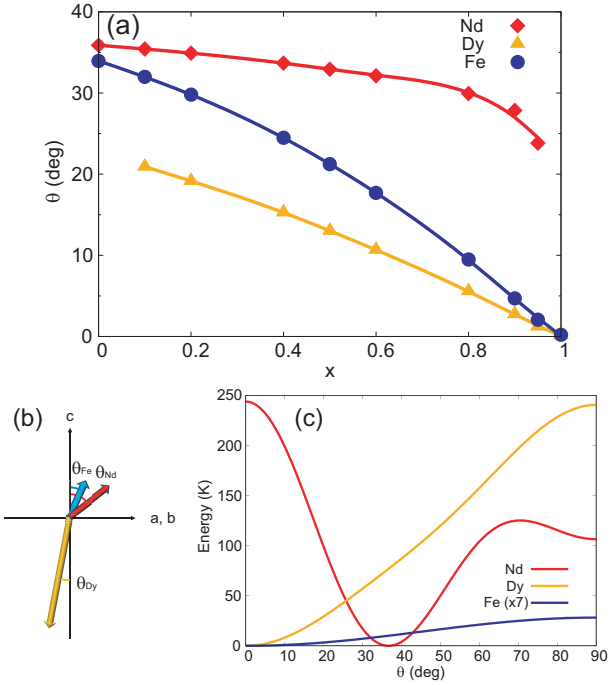

FIG. 7. (a) Concentration x dependence of the canting angle between the magnetic moment and c-axis for Fe, Dy, and Nd atoms. (b) Canting angles of Fe, Dy, and Nd atoms as a function of x. (c) Anisotropy energies as functions of the canting angle θ from the c axis for Nd, Dy, and Fe atoms. The anisotropy energy of Fe has been magnified seven times for clarity.

30–33 deg. at $T = 4.2\,\mathrm{K}$ [55]. Our simulation yields a canting angle of $\theta = 34$ deg. for $x = 0$, which is in good agreement with the experimental values.

The estimated value of θ decreases gradually with increasing x. Although our values are slightly larger than the experimental results reported by Lim et al. and Kim et al., they successfully capture the overall trend with respect to x. In the MF-like analysis by Lim et al., the canting angle of the magnetic moment decreases rapidly and disappears at $x \simeq 0.79$ as corresponding to their analysis of the x dependence of T_{SR}. However, in our result the cant of the moment remains at such large x and it gradually decrease toward $x = 1$. At $x = 0.75$, the experimental canting angle reported by Kim et al. is approximately $\theta \simeq 15$ deg. Compared to $\theta \simeq 6$ deg. from the MF-like model, our estimate of $\theta \simeq 18$ deg. is much closer to the experimental value. Considering both the x-dependences of T_{SR} and θ, our results suggest that T_{SR} does not vanish at $x \simeq 0.79$, making our estimation more consistent with experimental observations.

To investigate the canting behavior of the individual atomic moments, we present in Figs. 7(a) and (b) the concentration (x) dependence of the canting angle (θ) from the c axis for Nd, Dy, and Fe atoms at $T = 4\,\mathrm{K}$, estimated using the relation $\theta = \tan^{-1}\left(\frac{m_{xy}}{m_z}\right)$.

With a decrease of the Nd concentration (i.e., an increase of x), θ_{Nd} gradually decreases from $\theta = 36$ deg. and still maintain a large cant ($\simeq 27$ deg.) even at a very low Nd concentration such as $x = 0.9$. In contrast, θ_{Dy} shows a strong dependence on x. As the Dy concentration decreases (i.e., as x decreases), θ_{Dy} increases from $\theta = 0$ deg. and reaches approximately 22 deg. at $x = 0.1$.

θ_{Fe} exhibits the highest sensitivity to x among the three elements and takes values between θ_{Nd} and θ_{Dy}. As the concentration of Nd or Dy increases, θ_{Fe} tends to approach the corresponding value of θ_{Nd} or θ_{Dy}. These observations provides evidence that even at high x, the Nd moments remain canted at very low temperatures, thereby driving the SR transition.

We consider these canting angle dependencies from the perspective of the anisotropy energies of the constituent atoms. Figure 7(c) presents the per-site CEF energies for the rare-earth atoms (R=Nd or Dy), given by,

$$\mathcal{H}_{\mathrm{CEF}}(\mathrm{R}) = \sum_{l,m} \Theta_l A_l^m \langle r^l \rangle \hat{O}_l^m. \tag{7}$$

and per-site anisotropy energy (ground state energy) of Fe atoms, expressed as

$$\mathcal{H}_{\mathrm{a}} = -\frac{1}{N_{\mathrm{Fe}}} \sum_{i}^{\mathrm{Fe}} D_i (s_i^z)^2, \tag{8}$$

as a function of the angle θ. In both plots, the energy minimum is set to zero, and $\mathcal{H}_{\mathrm{a}}$ is multiplied by a factor of 7 for better visual clarity.

When only exchange interactions are considered, the total energy is minimized when $\theta_{\mathrm{Nd}} = \theta_{\mathrm{Fe}} = \theta_{\mathrm{Dy}} = 0$. However, the results discussed above suggest that this configuration is not energetically favorable due to the large CEF energy of Nd atoms, approximately $\mathcal{H}_{\mathrm{CEF}}(\mathrm{Nd}) \simeq 250$ K at $\theta_{\mathrm{Nd}} = 0$. Therefore, the actual minimum total energy is determined by a trade-off between the exchange interactions and the anisotropy energies of each atomic species. Since the CEF energy for Dy atoms and the anisotropy energy of Fe atoms have relatively shallow curvatures near their respective minima and increase gradually with θ, the system allows some deviation of Fe and Dy moments from their ideal alignment. Consequently, the Nd moments maintain a significant canting even at high Dy concentrations (x), enabling the SR transition to persist across a wide composition range.

C. Anomalous Behavior in Magnetization

In this subsection, we study the origin of the anomalous behavior in magnetization. In Figs. 8 (a), (b), and (c), temperature dependence of M is illustrated by a thick dashed line for $x = 0$, 0.4, and 0.8, respectively.

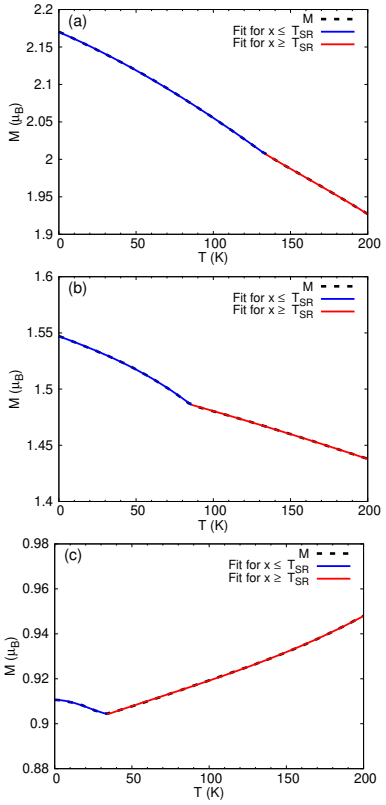

FIG. 8. Anomaly of the magnetization M of $(Nd_{1-x}Dy_x)_2Fe_{14}B$ systems for (a) $x = 0$, (b) $x = 0.4$, and (c) $x = 0.8$. The thick dashed curves represent the temperature dependence of M. The blue and red curves are fitted functions for $T \leq T_{SR}$ and $T \geq T_{SR}$, respectively.

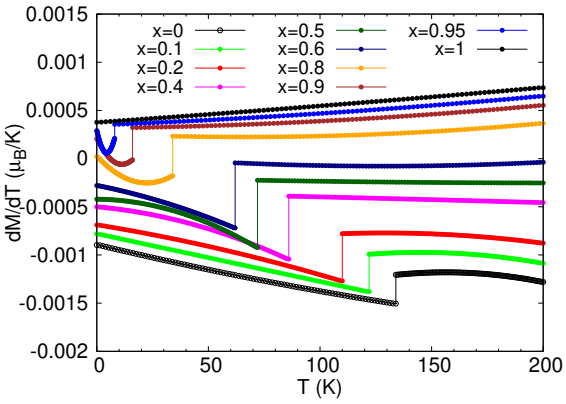

FIG. 9. Temperature dependences of $\frac{dM}{dT}$ for $(Nd_{1-x}Dy_x)_2Fe_{14}B$ systems.

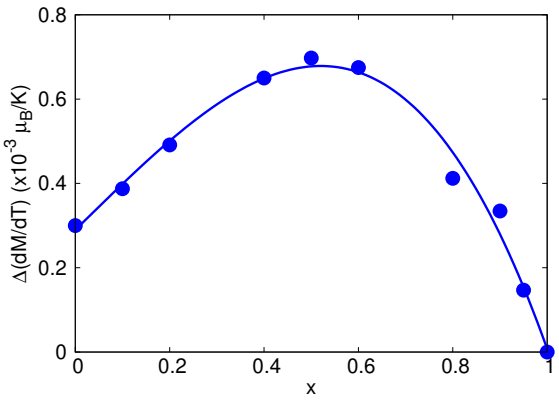

FIG. 10. Concentration (x) dependence of $\Delta\frac{dM}{dT}$ at T_{SR} for $(Nd_{1-x}Dy_x)_2Fe_{14}B$ systems.

The curves of M are well fitted by least-squares fits using cubic functions in the regions below and above T_{SR}, shown by blue and red lines, respectively. We observe a non-differentiable point in M at T_{SR} for $x = 0$, 0.4, and 0.8. In a similar manner, non-differentiable points at T_{SR} are found for all x values ($x \neq 0$). To quantify the degree of this anomaly, we evaluate dM/dT as a function of T with varying x.

Figure 9 shows dM/dT as a function of temperature for various values of x. Fig. 10 presents x dependence of the gap in dM/dT, defined as $\Delta dM/dT$ at T_{SR}. The solid line in Fig. 10 represents a cubic function fitted using the least-squares method. We find that as x increases from 0, the gap increases, reaches a maximum around $x = 0.5$, and then decreases toward $x = 1.0$. In the following, we examine the origin of this behavior.

In Figs. 11 (a), (b), and(c), the temperature dependences of m(Fe), m(Dy), and m(Nd) are plotted, respectively, for various values of x. We find that m exhibits no anomaly for Fe and Dy atoms, but a clear anomaly is observed for Nd atoms across all values of x. As x increases, m(Nd) smoothly extends toward lower temperatures and reaches T_{SR}, but shows a sharp increase below T_{SR}. Interestingly, this behavior becomes more pronounced with increasing x. It is also noteworthy that the magnitude of the Nd moment at absolute zero temperature remains nearly constant regardless of x. This indicates that the temperature at which the Nd moments exhibit anomalous behavior depends on the surrounding environment, specifically, the concentration of Dy atoms, but the ground-state magnitude of the Nd moment remains independent of the Dy concentration. As a result, the anomaly in the Nd moment at the SR transition temperature becomes more pronounced as the Dy concentration increases.

We estimate dm(Nd)$/dT$ as a function of T for all values of x. Following the same procedure as for estimating dM/dT, we find the temperature dependence of m(Nd) for all x is well described by least-squares fitting of cubic functions in the regions below and above T_{SR}. We

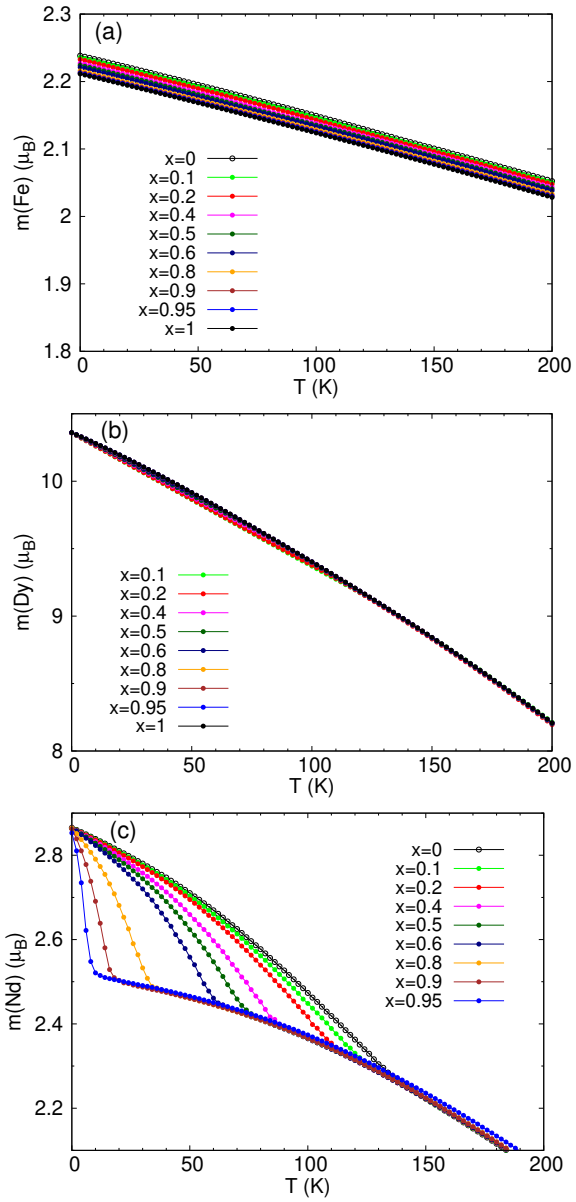

FIG. 11. Temperature dependences of (a) m(Fe) (b) m(Dy), and (c) m(Nd) for $(Nd_{1-x}Dy_x)_2Fe_{14}B$ systems.

thus obtain $dm(\mathrm{Nd})/dT$ from the slopes. We plot the gap of $dm(\mathrm{Nd})/dT$ at T_{SR}, denoted $\Delta dm(\mathrm{Nd})/dT$, as a function of x by blue circles in Fig. 12. We find that $\Delta dm(\mathrm{Nd})/dT$ increases rapidly increasing with x. Since $\Delta dm(\mathrm{Nd})/dT$ is a per-site quantity, the total gap for Nd atoms, denoted $\Delta(\mathrm{Nd})_{\mathrm{total}}$, is related by:

$$\Delta(\mathrm{Nd})_{\mathrm{total}} = N_{\mathrm{Nd}} \times \Delta\frac{dm(\mathrm{Nd})}{dT} \tag{9}$$

$$\propto (1-x) \times \Delta\frac{dm(\mathrm{Nd})}{dT}. \tag{10}$$

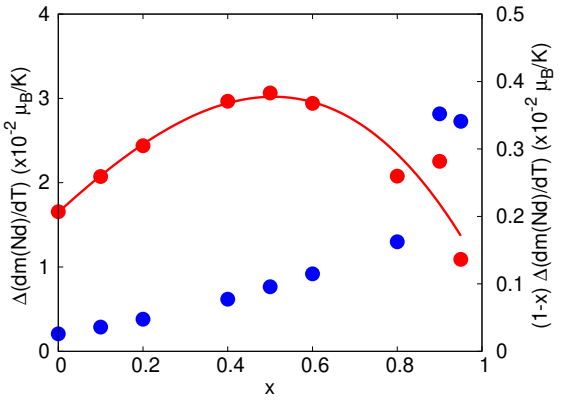

FIG. 12. Concentration (x) dependences of $\Delta\frac{dm(\mathrm{Nd})}{dT}$ (blue circles) and $\Delta\frac{dm(\mathrm{Nd})}{dT}(1-x)$ (red circles) at T_{SR} for $(Nd_{1-x}Dy_x)_2Fe_{14}B$ systems.

In Fig. 12, $(1-x) \times \Delta\frac{dm(\mathrm{Nd})}{dT}$ is given with red circles. The red solid line represents a cubic function fitted by the least-squares method. We find that the x dependence of $(1-x) \times \Delta dm(\mathrm{Nd})/dT$ at T_{SR} closely resembles that of $\Delta dM/dT$ at T_{SR}. Since the ratio of N_{Nd} to N (the total number of atoms) is $2(1-x) : 17$, the order of $\Delta\frac{dm(\mathrm{Nd})}{dT} \times \frac{2(1-x)}{17}$ is expected to be comparable to that of $\Delta dM/dT$. For example, $\Delta\frac{dm(\mathrm{Nd})}{dT} \times \frac{2(1-x)}{17} \simeq 0.47 \times 10^{-3}\mu_{\mathrm{B}}/\mathrm{K}$ for $x = 0.5$, which is the same order as $\Delta dM/dT \simeq 0.67 \times 10^{-3}\mu_{\mathrm{B}}/\mathrm{K}$ for $x = 0.5$. These considerations indicate that the origin of the anomaly in the total magnetization M lies in the behavior of the Nd magnetic moments, regardless of their concentration.

V. SUMMARY

Neodymium magnets ($Nd_2Fe_{14}B$) are important permanent magnets and are often employed with dysprosium substitution to enhance their coercive force. Therefore, it is important to study the magnetic properties of $(Nd_{1-x}Dy_x)_2Fe_{14}B$. In this work, we investigated the spin-reorientation (SR) transition in $(Nd_{1-x}Dy_x)_2Fe_{14}B$ using a recently developed atomistic modeling approach. This method treats microscopic details of magnetic interactions and temperature effects appropriately. We employed the Metropolis importance-sampling Monte Carlo method for the $(Nd_{1-x}Dy_x)_2Fe_{14}B$ model, using microscopic parameters primarily derived from first-principles calculations. We analyzed the temperature and concentration (x) dependences of the magnetization and its components under zero external field. Our simulations yielded the spin-reorientation transition temperature (T_{SR}) and canting angle (θ) of the total magnetization as functions of x that are in good agreement with experimental observations [54, 57]. We also found a sig-

nificant deviation in T_{SR} at high Dy concentrations (x) between our results and those of the mean-field (MF)-like theory by Lim et al. [54]. Based on our analysis of the canting angles and anisotropy energies of the constituent atoms, we conclude that our estimations provide a more physically reasonable description.

Furthermore, we investigated an anomalous feature in the magnetization near T_{SR}. We found that the anomaly in the total magnetization becomes more pronounced with increasing x, reaches a maximum at $x = 0.5$, and then diminishes for larger x. To elucidate the origin of this behavior, we analyzed the magnetic moments of the constituent atoms and identified the Nd moments as the primary source of the anomaly. As the Dy concentration increases, the temperature at which the Nd moment anomaly appears shifts to lower values. However, the magnitude of the Nd moment rapidly increases below T_{SR}, and at sufficiently low temperatures, it converges to nearly the same value for all x. In this regime, the canting angle of the Nd moments changes only slightly. Consequently, the anomaly in the Nd moment at T_{SR} becomes more significant with increasing Dy concentration, leading to the observed anomaly in the total magnetization M, which peaks at $x = 0.5$.

ACKNOWLEDGMENTS

The authors would like to thank Dr. Hirosawa for insightful discussions on the experimental results of $(Nd_{1-x}Dy_x)_2Fe_{14}B$, Prof. Miyashita for useful theoretical discussions, and Dr. Toga for helpful discussions on the magnetic parameters. This work was supported by Grants-in-Aid for Scientific Research B (No. 24K01332) from MEXT. Numerical calculations were performed using the Numerical Materials Simulator at the National Institute for Materials Science.

[1] M. Sagawa and S. Hirosawa, Magnetic hardening mechanism in sintered R–Fe–B permanent magnets, Journal of Materials Research **3**, 45 (1988).

[2] J. F. Herbst, J. J. Croat, F. E. Pinkerton, and W. B. Yelon, Relationships between crystal structure and magnetic properties in $Nd_2Fe_{14}B$, Phys. Rev. B **29**, 4176 (1984).

[3] S. Hirosawa, Y. Matsuura, H. Yamamoto, S. Fujimura, M. Sagawa, and H. Yamauchi, Single crystal measurements of anisotropy constants of $R_2Fe_{14}B$ (R=Y, Ce, Pr, Nd, Gd, Tb, Dy and Ho), Japanese Journal of Applied Physics **24**, L803 (1985).

[4] A. V. Andreev, A. V. Deriagin, N. V. Kudrevatykh, N. V. Mushnikov, and V. A. Reimer, The magnetism of $Y_2Fe_{14}B$ and $Nd_2Fe_{14}B$ and their hydrides, Zhurnal Eksperimentalnoi i Teoreticheskoi Fiziki **90**, 1042 (1986).

[5] H. Kronmüller, K.-D. Durst, and M. Sagawa, Analysis of the magnetic hardening mechanism in RE-FeB permanent magnets, Journal of Magnetism and Magnetic Materials **74**, 291 (1988).

[6] J. F. Herbst, $R_2Fe_{14}B$ materials: Intrinsic properties and technological aspects, Rev. Mod. Phys. **63**, 819 (1991).

[7] S. Hirosawa, Y. Matsuura, H. Yamamoto, S. Fujimura, M. Sagawa, and H. Yamauchi, Magnetization and magnetic anisotropy of $R_2Fe_{14}B$ measured on single crystals, Journal of Applied Physics **59**, 873 (1986).

[8] O. Yamada, Y. Ohtsu, F. Ono, M. Sagawa, and S. Hirosawa, Magnetocrystalline anisotropy in $Nd_2Fe_{14}B$ intermetallic compound, Journal of Magnetism and Magnetic Materials **70**, 322 (1987).

[9] P. B. Mushnikov, N. V.and Terent'ev and E. V. Rosenfel'd, Magnetic anisotropy of the $Nd_2Fe_{14}B$ compound and its hydride $Nd_2Fe_{14}BH_4$, The Physics of Metals and Metallography **103**, 39 (2007).

[10] T. Kohashi, K. Motai, T. Nishiuchi, and S. Hirosawa, Magnetism in grain-boundary phase of a NdFeB sintered magnet studied by spin-polarized scanning electron microscopy, Applied Physics Letters **104**, 232408 (2014).

[11] R. Friedberg and D. I. Paul, New Theory of Coercive Force of Ferromagnetic Materials, Phys. Rev. Lett. **34**, 1234 (1975).

[12] A. Sakuma, S. Tanigawa, and M. Tokunaga, Micromagnetic studies of inhomogeneous nucleation in hard magnets, Journal of Magnetism and Magnetic Materials **84**, 52 (1990).

[13] A. Sakuma, The theory of inhomogeneous nucleation in uniaxial ferromagnets, Journal of Magnetism and Magnetic Materials **88**, 369 (1990).

[14] S. Mohakud, S. Andraus, M. Nishino, A. Sakuma, and S. Miyashita, Temperature dependence of the threshold magnetic field for nucleation and domain wall propagation in an inhomogeneous structure with grain boundary, Phys. Rev. B **94**, 054430 (2016).

[15] S. Hirosawa, M. Nishino, and S. Miyashita, Perspectives for high-performance permanent magnets: applications, coercivity, and new materials, Advances in Natural Sciences: Nanoscience and Nanotechnology **8**, 013002 (2017).

[16] A. L. Wysocki and V. P. Antropov, Micromagnetic simulations with periodic boundary conditions: Hard-soft nanocomposites, Journal of Magnetism and Magnetic Materials **428**, 274 (2017).

[17] I. E. Uysal, M. Nishino, and S. Miyashita, Magnetic field threshold for nucleation and depinning of domain walls in the neodymium permanent magnet $Nd_2Fe_{14}B$, Phys. Rev. B **101**, 094421 (2020).

[18] S. Okamoto, R. Goto, N. Kikuchi, O. Kitakami, T. Akiya, H. Sepehri-Amin, T. Ohkubo, K. Hono, K. Hioki, and A. Hattori, Temperature-dependent magnetization reversal process and coercivity mechanism in Nd-Fe-B hot-deformed magnets, Journal of Applied Physics **118**, 223903 (2015).

[19] T. Pramanik, A. Roy, R. Dey, A. Rai, S. Guchhait, H. C. Movva, C.-C. Hsieh, and S. K. Banerjee, Angular dependence of magnetization reversal in epitaxial chromium telluride thin films with perpendicular mag-

netic anisotropy, Journal of Magnetism and Magnetic Materials **437**, 72 (2017).
[20] M. Nishino and S. Miyashita, Atomistic model study on magnetic properties of permanent magnets –treatment of thermal fluctuation and thermal effects, and future perspective–, MATERIALS TRANSACTIONS **66**, 1 (2025).
[21] K. Hirota, H. Nakamura, T. Minowa, and M. Honshima, Coercivity enhancement by the grain boundary diffusion process to Nd-Fe-B sintered magnets, IEEE Transactions on Magnetics **42**, 2909 (2006).
[22] F. Xu, J. Wang, X. Dong, L. Zhang, and J. Wu, Grain boundary microstructure in DyF3-diffusion processed nd-fe-b sintered magnets, Journal of Alloys and Compounds **509**, 7909 (2011).
[23] K. Löewe, C. Brombacher, M. Katter, and O. Gutfleisch, Temperature-dependent Dy diffusion processes in Nd-Fe-B permanent magnets, Acta Materialia **83**, 248 (2015).
[24] W. Chen, J. M. Luo, Y. W. Guan, Y. L. Huang, M. Chen, and Y. H. Hou, Grain boundary diffusion of Dy films prepared by magnetron sputtering for sintered Nd–Fe–B magnets, **51**, 185001 (2018).
[25] T.-H. Kim, T. Sasaki, T. Ohkubo, Y. Takada, A. Kato, Y. Kaneko, and K. Hono, Microstructure and coercivity of grain boundary diffusion processed Dy-free and Dy-containing Nd–Fe–B sintered magnets, Acta Materialia **172**, 139 (2019).
[26] S. Bance, J. Fischbacher, A. Kovacs, H. Oezelt, F. Reichel, and T. Schrefl, Thermal activation in permanent magnets, JOM **67**, 1350 (2015).
[27] J. Fischbacher, A. Kovacs, L. Exl, J. Kühnel, E. Mehofer, H. Sepehri-Amin, T. Ohkubo, K. Hono, and T. Schrefl, Searching the weakest link: Demagnetizing fields and magnetization reversal in permanent magnets, Scripta Materialia **154**, 253 (2018).
[28] H. Kronmüller and M. Fähnle, *Micromagnetism and the Microstructure of Ferromagnetic Solids*, Cambridge studies in magnetism (Cambridge University Press, 2003).
[29] G. Grinstein and R. H. Koch, Coarse graining in micromagnetics, Phys. Rev. Lett. **90**, 207201 (2003).
[30] R. J. Radwański and J. J. M. Franse, Rare-earth contribution to the magnetocrystalline anisotropy energy in $R_2Fe_{14}B$, Phys. Rev. B **36**, 8616 (1987).
[31] M. Ito, M. Yano, N. M. Dempsey, and D. Givord, Calculations of the magnetic properties of $R_2M_{14}B$ intermetallic compounds (R=rare earth, M=Fe, Co), Journal of Magnetism and Magnetic Materials **400**, 379 (2016).
[32] J. L. García-Palacios and F. J. Lázaro, Langevin-dynamics study of the dynamical properties of small magnetic particles, Phys. Rev. B **58**, 14937 (1998).
[33] M. Nishino and S. Miyashita, Realization of the thermal equilibrium in inhomogeneous magnetic systems by the Landau-Lifshitz-Gilbert equation with stochastic noise, and its dynamical aspects, Phys. Rev. B **91**, 134411 (2015).
[34] Y. Toga, M. Matsumoto, S. Miyashita, H. Akai, S. Doi, T. Miyake, and A. Sakuma, Monte Carlo analysis for finite-temperature magnetism of $Nd_2Fe_{14}B$ permanent magnet, Phys. Rev. B **94**, 174433 (2016).
[35] M. Nishino, Y. Toga, S. Miyashita, H. Akai, A. Sakuma, and S. Hirosawa, Atomistic-model study of temperature-dependent domain walls in the neodymium permanent magnet $Nd_2Fe_{14}B$, Phys. Rev. B **95**, 094429 (2017).
[36] T. Hinokihara, M. Nishino, Y. Toga, and S. Miyashita, Exploration of the effects of dipole-dipole interactions in $Nd_2Fe_{14}B$ thin films based on a stochastic cutoff method with a novel efficient algorithm, Phys. Rev. B **97**, 104427 (2018).
[37] S. Miyashita, M. Nishino, Y. Toga, T. Hinokihara, T. Miyake, S. Hirosawa, and A. Sakuma, Perspectives of stochastic micromagnetism of $Nd_2Fe_{14}B$ and computation of thermally activated reversal process, Scripta Materialia **154**, 259 (2018).
[38] Y. Toga, M. Nishino, S. Miyashita, T. Miyake, and A. Sakuma, Anisotropy of exchange stiffness based on atomic-scale magnetic properties in the rare-earth permanent magnet $Nd_2Fe_{14}B$, Phys. Rev. B **98**, 054418 (2018).
[39] M. Nishino and S. Miyashita, Nontrivial temperature dependence of ferromagnetic resonance frequency for spin reorientation transitions, Phys. Rev. B **100**, 020403 (2019).
[40] Y. Toga, S. Miyashita, A. Sakuma, and T. Miyake, Role of atomic-scale thermal fluctuations in the coercivity, npj Computational Materials **6**, 67 (2020).
[41] M. Nishino, I. E. Uysal, T. Hinokihara, and S. Miyashita, Dynamical aspects of magnetization reversal in the neodymium permanent magnet by a stochastic Landau-Lifshitz-Gilbert simulation at finite temperature: Real-time dynamics and quantitative estimation of coercive force, Phys. Rev. B **102**, 020413(R) (2020).
[42] S. Westmoreland, R. Evans, G. Hrkac, T. Schrefl, G. Zimanyi, M. Winklhofer, N. Sakuma, M. Yano, A. Kato, T. Shoji, A. Manabe, M. Ito, and R. Chantrell, Multiscale model approaches to the design of advanced permanent magnets, Scripta Materialia **148**, 56 (2018).
[43] S. C. Westmoreland, C. Skelland, T. Shoji, M. Yano, A. Kato, M. Ito, G. Hrkac, T. Schrefl, R. F. L. Evans, and R. W. Chantrell, Atomistic simulations of α-$Fe/Nd_2Fe_{14}B$ magnetic core/shell nanocomposites with enhanced energy product for high temperature permanent magnet applications, Journal of Applied Physics **127**, 133901 (2020).
[44] Q. Gong, M. Yi, R. F. L. Evans, B.-X. Xu, and O. Gutfleisch, Calculating temperature-dependent properties of $Nd_2Fe_{14}B$ permanent magnets by atomistic spin model simulations, Phys. Rev. B **99**, 214409 (2019).
[45] Q. Gong, M. Yi, and B.-X. Xu, Multiscale simulations toward calculating coercivity of Nd–Fe–B permanent magnets at high temperatures, Phys. Rev. Materials **3**, 084406 (2019).
[46] Q. Gong, M. Yi, R. F. L. Evans, O. Gutfleisch, and B.-X. Xu, Anisotropic exchange in Nd–Fe–B permanent magnets, Materials Research Letters **8**, 89 (2020).
[47] S. Miyashita, M. Nishino, Y. Toga, T. Hinokihara, I. E. Uysal, T. Miyake, H. Akai, S. Hirosawa, and A. Sakuma, Atomistic theory of thermally activated magnetization processes in $Nd_2Fe_{14}B$ permanent magnet, Science and Technology of Advanced Materials **22**, 658 (2021).
[48] M. Nishino, I. E. Uysal, and S. Miyashita, Effect of the surface magnetic anisotropy of neodymium atoms on the coercivity in neodymium permanent magnets, Phys. Rev. B **103**, 014418 (2021).
[49] M. Nishino, H. Hayasaka, and S. Miyashita, Microscopic origin of coercivity enhancement by dysprosium substitution into neodymium permanent magnets, Phys. Rev. B **106**, 054422 (2022).

[50] H. Hayasaka, M. Nishino, and S. Miyashita, Microscopic study on the angular dependence of coercivity at zero and finite temperatures, Phys. Rev. B **105**, 224414 (2022).

[51] M. Nishino and S. Miyashita, Quantitative estimation of coercive field in a ferromagnetic grain using field sweep simulation, Phys. Rev. B **107**, 184422 (2023).

[52] M. Nishino, H. Hayasaka, and S. Miyashita, Thermodynamic properties of $R_2Fe_{14}B$ (R=Dy, Nd) and dysprosium random substitution effect on coercivity in neodymium permanent magnets, Journal of Applied Physics **136**, 033904 (2024).

[53] M. Yamada, H. Kato, H. Yamamoto, and Y. Nakagawa, Crystal-field analysis of the magnetization process in a series of $Nd_2Fe_{14}B$-type compounds, Phys. Rev. B **38**, 620 (1988).

[54] D. W. Lim, H. Kato, M. Yamada, G. Kido, and Y. Nakagawa, High-field magnetization process and spin reorientation in $(Nd_{1-x}Dy_x)_2Fe_{14}B$ single crystals, Phys. Rev. B **44**, 10014 (1991).

[55] Y. Kim, M. Kim, J. Hur, and T. Kim, Effects of powder alignment on determination error of spin reorientation angle of cone anisotropy, Journal of Magnetism and Magnetic Materials **195**, 741 (1999).

[56] C. Piqué, R. Burriel, and J. Bartolomé, Spin reorientation phase transitions in R2Fe14B (R = Y, Nd, Ho, Er, Tm) investigated by heat capacity measurements, Journal of Magnetism and Magnetic Materials **154**, 71 (1996).

[57] M. Kim, Y. Kim, C. Kim, and T. Kim, Spin reorientation and magnetocrystalline anisotropy of $(Nd_{1-x}Dy_x)_2Fe_{14}B$, Journal of Magnetism and Magnetic Materials **224**, 49 (2001).

[58] J. Soler-Morala, I. Arnay, G. Gkouzia, P. Pedraz, P. Perna, L. Alff, C. Navío, and A. Bollero, Spin reorientation transition in epitaxial nanometric Nd-Fe-B films with large perpendicular magnetic anisotropy, Journal of Alloys and Compounds **1006**, 176215 (2024).

[59] W. B. Yelon, B. Foley, C. Abache, and H. Oesterreicher, Spin reorientation in NdDyFe14B, Journal of Applied Physics **60**, 2982 (1986).

[60] `http://kkr.issp.u-tokyo.ac.jp/`.

[61] A. Liechtenstein, M. Katsnelson, V. Antropov, and V. Gubanov, Local spin density functional approach to the theory of exchange interactions in ferromagnetic metals and alloys, Journal of Magnetism and Magnetic Materials **67**, 65 (1987).

[62] See supplemental material at XXX, which includes Refs. [53, 60, 64, and 65], for details of the atomistic model parameters.

[63] T. Miyake, Y. Harashima, T. Fukazawa, and H. Akai, Understanding and optimization of hard magnetic compounds from first principles, Science and Technology of Advanced Materials **22**, 543 (2021).

[64] A. J. Freeman and R. E. Watson, Theoretical Investigation of Some Magnetic and Spectroscopic Properties of Rare-Earth Ions, Phys. Rev. **127**, 2058 (1962).

[65] Y. Miura, H. Tsuchiura, and T. Yoshioka, Magnetocrystalline anisotropy of the Fe-sublattice in $Y_2Fe_{14}B$ systems, Journal of Applied Physics **115**, 17A765 (2014).